Synergy between Ni$_3$Sn$_2$ alloy and Lewis acidic ReO$_x$ enables selectivity control of furfural hydrogenation to cyclopentanone

Wei Lin [a,1], Yuexing Zhang [c,1], Zixu Ma [a], Zhiwei Sun [a], Xiaolong Liu [b,*], Chunbao Charles Xu [d], Renfeng Nie [a,*]

[a] National Key Laboratory of Biobased Transportation Fuel Technology, School of Chemical Engineering, Henan Center for Outstanding Overseas Scientists, Zhengzhou University, Zhengzhou 450001, China
[b] CAS Key Laboratory of Green Process and Engineering, Institute of Process Engineering, Chinese Academy of Sciences, Beijing 100190, China
[c] College of Chemistry and Chemical Engineering, Dezhou University, Dezhou 253023, China
[d] School of Energy and Environment, 580 City University of Hong Kong, Kowloon, Hong Kong Special Administrative Region

ARTICLE INFO

ABSTRACT

Selectivity controlling is a crucial and challenging issue for the hydrogenation of furfural (FAL) to cyclopentanone (CPO). Herein, Ni$_3$Sn$_2$-ReO$_x$/TiO$_2$ is synthesized via successive impregnation and exhibits full conversion and 92.5 % CPO selectivity under 3.0 MPa H$_2$ at 140 °C, which are much higher than those of Ni/TiO$_2$ and Ni$_3$Sn$_2$/TiO$_2$. Characterizations show that Ni$_3$Sn$_2$ is the main active phase that remarkably restrains the over-hydrogenation of the furan ring, while ReO$_x$ plays an electrophile or Lewis acid site to activate C-OH of furfuryl alcohol and induces its rearrangement. DFT calculations verify that Sn doping weakens the furan ring adsorption on Ni$_3$Sn$_2$ and shifts its adsorption configuration, which consequently inhibits side reactions and favors the metal-acid (Ni$_3$Sn$_2$-ReO$_x$) synergy. The catalyst is stable, recyclable and also active at even 0.5 MPa H$_2$ and 80 °C. This study provides an advanced strategy for the rational design of superior catalysts for tuning product selectivity, with practical potential for upgrading biomass-derived platform molecules.

1. Introduction

Cyclopentanone (CPO) is a versatile chemical intermediate that can be used for the synthesis of fungicides, pharmaceuticals, rubber chemicals, and flavours and fragrances [1,2]. Traditionally, CPO can be prepared by the catalytic vapor-phase cyclization of 1,6-hexanediol [3, 4] or adipic acid esters [5,6] or by the liquid phase oxidation of cyclopentene with nitrous oxide [7,8], which is accompanied by complex and polluting production processes, poor yield of CPO and strong dependency on nonrenewable fossil resources. Therefore, it is urgent to develop a green environment-friendly routine for sustainable CPO production.

Biomass, a globally available, renewable and natural carbon resource, can be converted into renewable fuels and chemicals [9–12]. Among these biomass-derived chemicals, furan derivatives, e.g., furfural (FAL), are readily acquired [13]. FAL can be converted into a range of nonpetroleum-derived chemicals, including CPO. Catalytic transformation of FAL to CPO involves several steps: (1) FAL is hydrogenated

to furfuryl alcohol (FOL) with C=O reduced to C–OH; (2) FOL is rearranged to 4-hydroxy-2-cyclopentenone (HCP); (3) HCP is dehydrated and hydrogenated to CPO with the removal of the hydroxyl group and hydrogenation of C=C bond. The above processes involve both the hydrogenation and acid-catalysis steps [14,15], which thus require the co-existence of both the metal sites for the hydrogenation reactions and the acidic sites for the acid-catalyzed reactions.

Up to now, there have been plenty of catalysts reported for the hydrogenation of FAL to CPO, many of which are noble metal-based catalysts, such as Ru [16], Pd [17,18] and Pt [19]. However, the high costs and low reserves of noble metals limit their widespread applications. In terms of non-noble metals, numerous investigations have been performed for the selective hydrogenation of FAL over supported metal catalysts including Cu [20–22], Ni [23–25] and Co [26–28] due to their acceptable catalytic activity. Based on previous studies, the sintering of metallic copper species, especially in an aqueous medium, is a major obstacle to its industrial application [29]. Nickel catalyst generally is more resistant to sintering than copper catalyst [28], but it favors

over-hydrogenation of the furan ring in FAL hydrogenation due to the preference for the binding of furan ring onto its surface [30]. On the other hand, the over-hydrogenation of carbonyl in CPO is also uncontrollable on Ni and Cu metals [25,31], which inevitably diminishes the CPO selectivity. Therefore, it is urgent to design highly efficient catalytic systems for selective FAL hydrogenation featuring high stability as well as greatly improved activity and selectivity.

Considering the reported catalysts, improved catalytic activity and selectivity for FAL hydrogenation can be obtained by modulating the hydrogenation sites and the acidic sites. In this aspect, the introduction of the second metal to form bimetallic catalysts (e.g., PdCu [32], PdCo [33], CuCo [34], CuNi [2,35], CuZn [36] and NiMo [37]) that can achieve a synergetic effect. For instance, the introduction of Cu can influent the electronic structure of Ni and favor the transformation of the FAL adsorption orientation, thus contributing to improved catalytic selectivity compared to monometallic Ni or Cu catalysts [35]. On the other hand, the balanced distribution of the acidic sites is also of great importance for selectively converting furfural to CPO. Generally, Acidic components or supports (such as alumina [31], pyrochlore [18], MOFs [16,33], NiO [23], Cu$_2$O [34] and phosphate [38]) have important effect on the reaction. A Lewis acid promotes the synthesis of the target product by ring-opening and intramolecular aldol reactions, and a Brønsted acid easily triggers the generation of macromolecular humins via the intermolecular coupling reaction of active intermediates [39]. For instance, Cu$_2$O played an electrophile or Lewis acid site to polarize the C-O bond via lone pair electrons on oxygen [34], thus favoring the rearrangement of the furan ring and promoting the formation of CPO. Moreover, the locations of metal sites and acid sites are spatially separated over conventional catalysts, thus resulting in a slow transport rate of intermediates from metal to acid sites and leading to low productivity of the target products even under harsh reaction conditions [40]. Therefore, although great progress has been made, it is still necessary to develop efficient bifunctional catalysts that with well-defined metal sites, balanced acid sites and intimate hydrogenation-acid sites for the selective conversion of FAL to CPO.

Herein, we report the catalytic conversion of FAL to CPO, applying supported NiSn-ReO$_x$ catalysts prepared by the continuous impregnation method. The reason for incorporating Sn into the Ni catalysts is that NiSn catalysts have been the most widely used to achieve selective hydrogenation of the C=O bond while leaving the C=C bonds in the furan nucleus intact [41]. Moreover, ReO$_x$ acts as Lewis acid sites or electrophilic sites due to the unsaturated coordination state, which has been successfully used as a promotor for C-O bond activation of biomass [42]. The effects of Ni/Sn ratio, acidity, reaction time and hydrogen pressure on the distribution of CPO, CPL and other products were studied. Finally, the surface area, metal composition, surface morphology and acidity were characterized by BET, XPS, XRD, TEM and NH$_3$-TPD, and the reaction process and mechanism were also discussed.

2. Experimental

2.1. Materials

Nickel nitrate hydrate (Ni(NO$_3$)$_2$·6H$_2$O, ≥ 98 %) and n-heptane (≥ 98.5 %) were purchased from Tianjin Fengchuan Chemical Reagent Technology Co., Ltd. Ammonium perrhenate (NH$_4$ReO$_4$, ≥99 %), SnCl$_4$·5H$_2$O (≥98 %), furfural (FAL, ≥99 %), tetrahydrofurfuryl alcohol (THFOL, ≥98 %), cyclopentanone (CPO, ≥98 %), cyclopentanol (CPL, ≥98 %) were purchased from Shanghai Macklin Biochemical Co., Ltd. Furfuryl alcohol (FOL, ≥98 %) was purchased from Shanghai Aladdin Biochemical Technology Co., Ltd. Gas phase titanium dioxide (P25) was purchased from Shaoxing Lijie Chemical Co., Ltd. All other chemicals were of analytical purity if not otherwise noted.

2.2. Catalyst synthesis

Synthesis of Ni/TiO$_2$. Ni(NO$_3$)$_2$·6H$_2$O (3.4 mmol) and TiO$_2$ (2.0 g) were added into 100 mL distilled water and stirred at room temperature for 1 h. The solid sample was obtained after removing water in a rotary evaporator, and the powder was dried in a vacuum oven at 60 °C for 12 h. Then the sample was reduced in H$_2$ atmosphere at 400 °C for 1 h in a tubular furnace and passivated in O$_2$/N$_2$ (1.5/98.5, v/v) atmosphere for 1 h at room temperature, yielding the Ni/TiO$_2$ catalyst with about 10 % Ni content.

Synthesis of Ni$_3$Sn$_2$/TiO$_2$. Ni(NO$_3$)$_2$·6H$_2$O (3.44 mmol), SnCl$_4$·5H$_2$O (1.14 mmol) and TiO$_2$ (2.0 g) were added into 100 mL ethanol and stirred at room temperature for 1 h. The solid sample was obtained after removing water in a rotary evaporator, and the powders were dried in a vacuum oven at 60 °C for 12 h. The obtained solid was calcinated in a muffle furnace at 400 °C for 4 h, then reduced in H$_2$ atmosphere at 400 °C for 1 h in a tubular furnace and passivated in O$_2$/N$_2$ (1.5/98.5, v/v) atmosphere for 1 h at room temperature, yielding the catalyst named as Ni$_3$Sn$_2$/TiO$_2$.

Synthesis of Ni$_3$Sn$_2$-ReO$_x$/TiO$_2$. One gram of Ni$_3$Sn$_2$/TiO$_2$ catalyst was added to 100 mL distilled water with 0.27 mmol NH$_4$ReO$_4$ and stirred at room temperature for 1 h. The solid sample was obtained after removing water in a rotary evaporator, and the powders were dried in a vacuum oven at 60 °C for 12 h. The sample was reduced at 200 °C in H$_2$ atmosphere for 1 h in a tube furnace and passivated in O$_2$/N$_2$ (1.5/98.5, v/v) atmosphere for 1 h at room temperature, yielding the catalyst named as Ni$_3$Sn$_2$-ReO$_x$/TiO$_2$. Moreover, Ni-ReO$_x$/TiO$_2$ catalyst was prepared by loading ReO$_x$ on Ni/TiO$_2$ via a similar method as above, and the Re loading was consistent with that of Ni$_3$Sn$_2$-ReO$_x$/TiO$_2$.

2.3. Characterizations

Powder X-ray diffraction (XRD) was performed on a Panalytic Empyrean diffractometer and analyzed using Cu Kα radiation sources (45KV and 40 mA) in the 2θ range of 5–90°. Raman spectra were collected at room temperature using 514.5 nanometer Ar ion lasers (Renishaw Instruments) in the range of 100–4000 cm^{-1}. N$_2$ physisorption was carried out at −196 °C using the ASAP2460 autoadsorption analyzer (Micromeritics). Before adsorption measurements were taken, the samples were degassed at 250 °C overnight. The total pore volume was determined from the aggregation of N$_2$ vapor adsorbed at a relative pressure of 0.99. The specific surface area was calculated using the BET method, and the pore size was estimated using BJH method from the desorption branch of the isotherms. X-ray photoelectron spectra (XPS) were recorded on a Kratos XSAM 800 system. The binding energy values were strictly calibrated using the C1s peak at 284.6 eV. The contents of Ni, Sn and Re were determined by Thermo Scientific iCAP PRO X inductively coupled plasma-optical emission spectroscopy (ICP-OES). Scanning electron microscopy (SEM) images were recorded on SUPRA55. Transmission electron microscopy (TEM) images were obtained using an accelerating voltage of 200 kV on a JEOL-135 2010F Transmission Electron Microscope. Scanning TEM (STEM) images were recorded using the FEI Titan G260–300 Transmission Electron Microscope operated at 200 kV. Adsorption of CPO on the catalyst was measured by UV–vis (SHIMADZU UV-2600).

The chemisorption was performed on Auto Chem II 2920 (Micromeritics, USA) equipped with a thermal conductivity detector (TCD). Before the measurement, 200 mg catalyst was pretreated at 200 °C for 1 h in an Ar flow of 20 mL/min and then cooled down to 50 °C. As for H$_2$ or NH$_3$-TPD, the sample was treated with 10 % H$_2$/Ar or NH$_3$ (15 mL/min) for 60 min and swept with Ar (20 mL/min) for 60 min. Subsequently, the sample was heated to 600 °C with a heating rate of 10 °C/min under Ar (15 mL/min).

CO-FTIR measurements were performed over Thermo Fisher (iS50, US) infrared spectrometer in a transmission reactor. The sample was pretreated in a reactor with H$_2$ at 200 °C for 1 h, then cooled to room
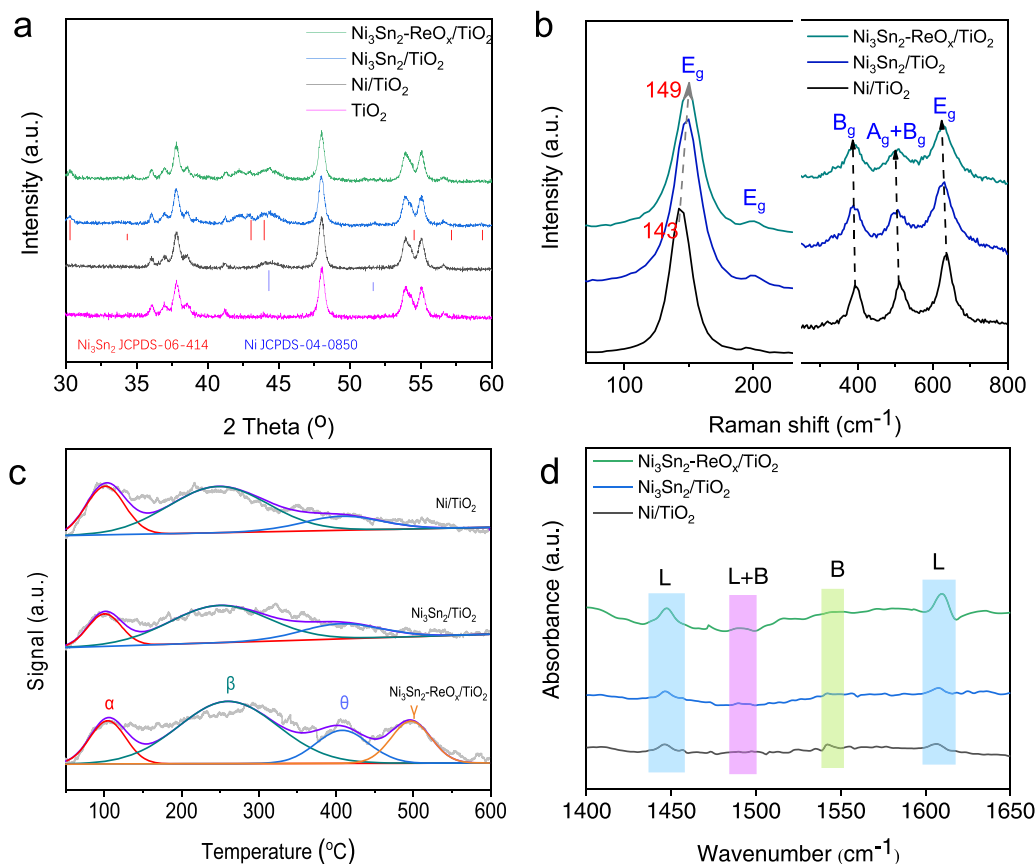
Fig. 1. (a) XRD patterns, (b) Raman, (c) NH$_3$-TPD and (d) Py-FTIR spectra of Ni/TiO$_2$, Ni$_3$Sn$_2$/TiO$_2$ and Ni$_3$Sn$_2$-ReO$_x$/TiO$_2$ catalysts.

temperature in H$_2$ flow to acquire the reference signal. Subsequently, 1 % CO/N$_2$ was introduced for 30 min, followed by a collection of infrared signals. In the case of FAL adsorption, the sample was pretreated in H$_2$ flow at 200 °C for 1 h, then cooled to room temperature. Then FAL was introduced into the reactor for 15 min; and N$_2$ was purged to remove the physically adsorbed molecule followed by collection of IR signals.

In the Py-FTIR test, 15 mg of catalyst and 15 mg of potassium bromide were pressed and fixed in the sample cell. The sample cell was pretreated at 300 °C for 1 h in vacuum and then cooled to 30 °C to introduce gaseous pyridine. After adsorption for 1 h, the samples were treated at 50 °C, 100 °C, and 150 °C for 1 h, respectively.

2.4. Computational methods

The bulk Ni and Ni$_3$Sn$_2$ crystal structures were built using the Materials Visualizer interface of BIOVIA Materials Studio 2017 (17.2), then these structures along with the cell unit were optimized. The Perdew-Burke-Ernzerh exchange-correlation functional of generalized gradient approximation (GGA-PBE) with Grimme's default DFT-D parameters was used. The double-numeric with polarization functions basis set (DNP) was chosen. All calculations were performed using the DMol^3 module of BIOVIA Materials Studio 2017 (17.2). The optimized crystal of Ni is FM-3 M space group with $a=b=c=3.520$ Å and $\alpha = \beta = \gamma = 90°$, while Ni$_3Sn_2$ crystal is optimized to PNMA space group with $a = 7.098$ Å, $b = 5.3325$ Å, $c = 8.3326$ Å, $\alpha = \beta = \gamma = 90°$. Ni(111) and Ni$_3Sn_2$(110) surfaces are cleaved based on the optimized crystals by adding 30 Å vacumm layer in c axis direction. After geometry optimization (cell parameters are fixed), the crystal parameters of Ni(111) and Ni$_3$Sn$_2$(110) surfaces are $a=b=9.9548$ Å, $c = 34.0640$ Å, $\alpha = \beta = 90°$, and $\gamma = 120°$ for the former and $a = 10.9460$ Å, $b = 10.6650$ Å, $c = 40.3267$ Å, $\alpha = \beta = \gamma = 90°$ for the latter. The cell and the inter-layer atoms are constrained when optimizing the complicated adsorption

systems. The convergence criteria for structure optimization were set to (a) an SCF tolerance of 1×10^{-5} Hartree, (b) an energy tolerance of 1×10^{-5} Hartree, (c) a maximum force tolerance of 2×10^{-3} Hartree/Å; and (d) a maximum displacement tolerance of 5×10^{-3} Å, (e) thermal smearing of 0.010 Ha, and (f) Monkhorst-Pack grid k-points of $1 \times 1 \times 1$. Based on the optimized crystal structures, adsorption energies were performed with a similar setup as optimization.

2.5. Catalyst test

The selective hydrogenation of FAL was carried out in a PSK–6–10 mL micro-magnetic heating reactor (Nanjing Zhengxin Instrument Co., Ltd.). Catalyst (50 mg), furfural (1 mmol) and H$_2$O (3.5 mL) and n-heptane (internal standard, 1 mmol) were added into stainless steel autoclave (10 mL). The high-pressure reactor was purged and discharged with 1 MPa H$_2$ five times and then filled with hydrogen to the specified pressure. The autoclave was then heated to the required temperature for the reaction. After the reaction, the reactor was quickly quenched in cold water, the solid catalyst was separated by centrifugation. The liquid was analyzed by gas chromatography (SHIMADZU GC-2010, flame ionization detector). The conversion rate and product selectivity of furfural were calculated by the following formula:
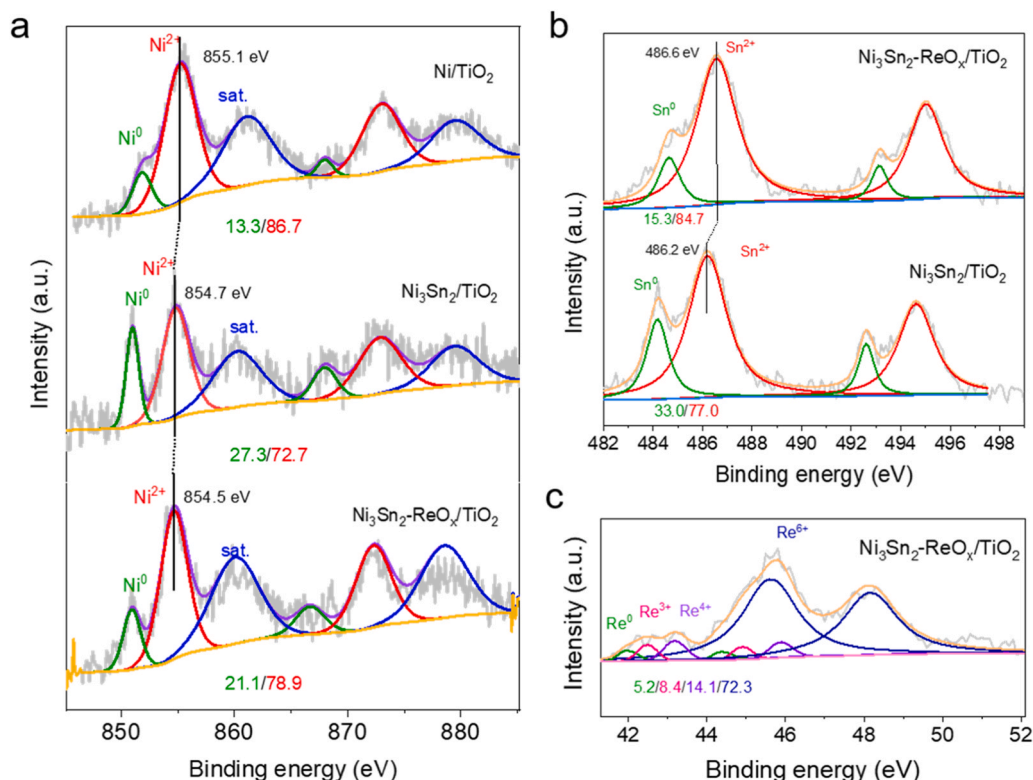
$$\text{Conversion}(\%) = \left(1 - \frac{\text{Molar amount of FAL after reaction}}{\text{Initial molar amount of FAL fed}} \right) \times 100\% \quad (1)$$

$$\text{Selectivity}(\%) = \frac{\text{Molar amount of one product}}{\text{Total molar amount of FAL converted}} \times 100\% \quad (2)$$

$$\text{Yield}(\%) = \frac{\text{Molar amount of one product}}{\text{Initial molar amount of FAL fed}} \times 100\% \quad (3)$$

Table 1
Catalytic hydrogenation of FAL over different Ni-based catalysts.[a]

FAL → **FOL** + **THFOL** + **CPO** + **CPL** + others.

Entry	Catalyst	t (h)	Conv. (%)	Yield (%)				
				FOL	THFOL	CPO	CPL	Others
1	Ni/TiO₂	3	100	0	68.5	11.5	15.3	4.7
2	Ni₃Sn₂/TiO₂	3	65.6	20.7	0	40.8	0	4.1
3	Ni₃Sn₂-ReOₓ/TiO₂	3	89.1	12.8	0	72.5	0	3.8
4	Ni-ReOₓ/TiO₂	3	100	0	41.2	0	54.7	4.1
5	Ni/TiO₂	6	100	0	70.2	0	24.8	5
6	Ni₃Sn₂/TiO₂	6	90.9	24.4	0	61.1	0	5.4
7	Ni₃Sn₂-ReOₓ/TiO₂	6	100	0	0	92.5	1	6.5

[a] Reaction conditions: FAL (1 mmol), catalyst (50 mg), H_2O (3.5 mL), H_2 (3 MPa), 140 °C.

Fig. 2. XPS spectra of (a) Ni 2p, (b) Sn 3d and (c) Re 4 f of Ni/TiO₂, Ni₃Sn₂/TiO₂ and Ni₃Sn₂-ReOₓ/TiO₂ catalysts.

3. Results and discussions

3.1. Catalyst characterizations

XRD analysis was applied to characterize the crystalline structure of the synthesized catalysts. As shown in Fig. 1a, Ni/TiO₂ only exhibits Ni (111) crystal plane at 44.5°. As for Ni₃Sn₂/TiO₂ and Ni₃Sn₂-ReOₓ/TiO₂, the diffraction peaks at 43.5° and 44.4° can be classified into Ni₃Sn₂(102) and Ni₃Sn₂(110) crystal planes (JCPDS-35–1362), respectively, indicating the Ni₃Sn₂ is the main metal phase in Ni₃Sn₂/TiO₂ and Ni₃Sn₂-ReOₓ/TiO₂. Compared with Ni₃Sn₂/TiO₂, doping ReOₓ does not change the crystal phase of NiSn in Ni₃Sn₂-ReOₓ/TiO₂. Moreover, the diffraction peaks of Re species are unobservable in Ni₃Sn₂-ReOₓ/TiO₂, indicating that Re species could be highly dispersed on the support. As shown in Raman spectra (Fig. 1b), six peaks at around 142 (Eg), 194 (Eg), 395 (Bg), 510 (Ag + Bg) and 634 cm⁻¹ (Eg) are detected in all samples, ascribing to Raman-active modes of anatase [43]. The position of the Eg peak in Ni₃Sn₂-ReOₓ/TiO₂ shifts to higher energy compared with that of

Ni/TiO₂ because of the strong interaction between Sn, ReOₓ and TiO₂ that restrains the bending vibration of O–Ti–O bond [44]. All samples show rich mesopore structure (Fig. S1), and the surface area and pore volume of Ni-based catalysts keep constant at ~45 m²/g and ~0.30 cm³/g, respectively (Table 1 and Table S1).

NH₃-TPD was used to investigate the effect of Sn and Re species on the acidity of Ni-based catalysts (Fig. 1c, Table S2). The Ni/TiO₂ shows three overlapping peaks at 100 (α), 260 (β) and 400 °C (γ) in the range of weak to medium acidity, attributing to acidity originating from unsaturated Ti⁴⁺ ions of TiO₂. After the introduction of Sn on Ni/TiO₂, the γ peak shifts to 300 °C, and the acidity of Ni₃Sn₂/TiO₂ is similar to that of mono-metallic Ni/TiO₂. Further introducing ReOₓ results in the shifting of the γ peak to 400 °C and the appearance of a new-born λ peak (strong acidity) at 500 °C, indicating that ReOₓ enhances the acidity of the Ni₃Sn₂-ReOₓ/TiO₂. Py-FTIR was adopted to further check the acid type of the catalysts (Fig. 1d, Table S2). Peak integration indicates that Lewis acid accounts for the majority of all acid sites for all samples, while minor Bronsted acid keeps almost constant. For instance, the Lewis acid
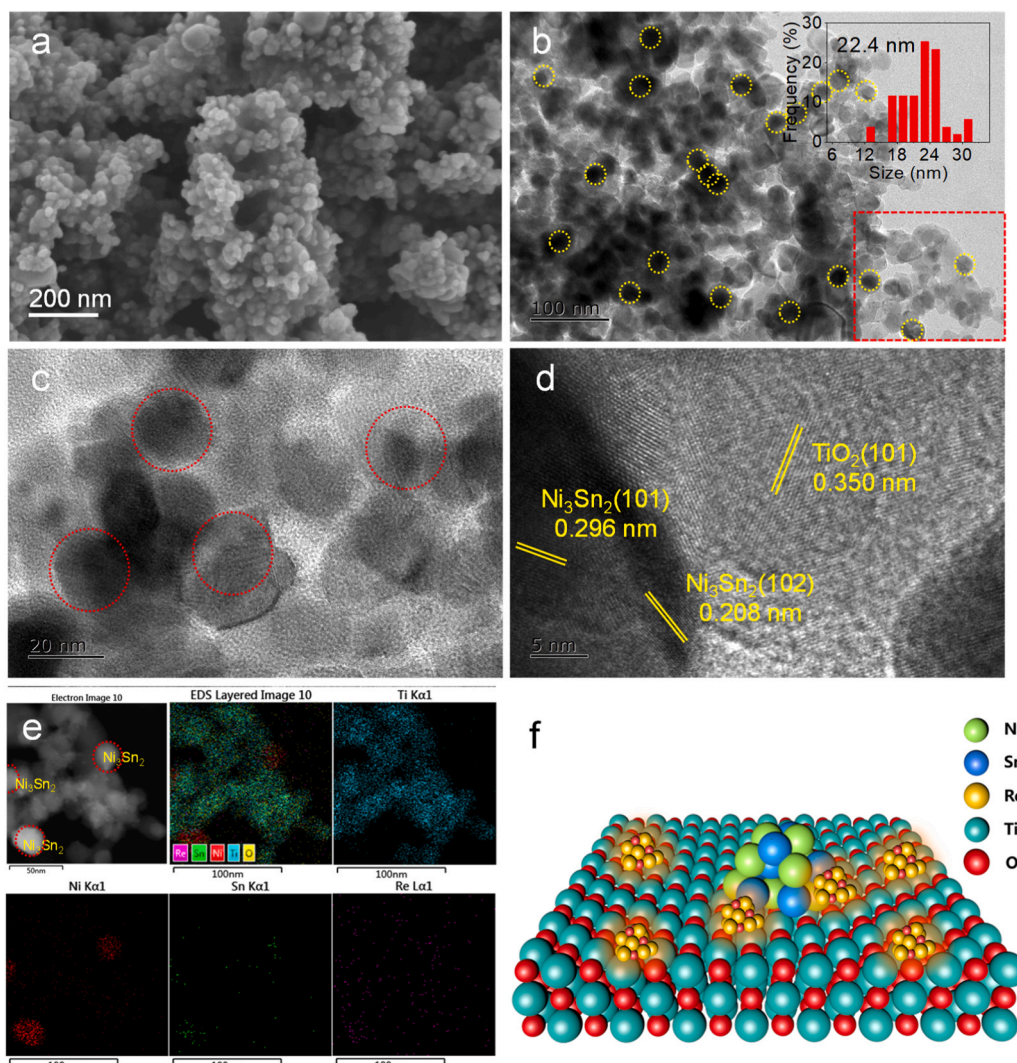
Fig. 3. (a) SEM image, (b-d) TEM images, (e) EDS element mappings and (f) structure model of Ni_3Sn_2-ReO_x/TiO_2.

density of Ni_3Sn_2-ReO_x/TiO_2 is calculated to be 28.3 μmol/g, which is much higher than those of Ni/TiO_2 (11.6 μmol/g) and Ni_3Sn_2/TiO_2 (12.3 μmol/g). These results reveal that ReO_x doping introduces rich Lewis acid in Ni_3Sn_2-ReO_x/TiO_2.

The surface structure and composition of the catalysts were studied by XPS (Fig. 2 and S2, Table S3 and S4). The fitting results of Ni 2p XPS spectra (Fig. 2a) show that the Ni species on the surface of TiO_2 are mainly oxidized, although XRD results show that they mainly exist in metal state, which is because the surface of metal Ni NPs is highly oxidized to the oxidized state by oxygen whether in passivation process or gas storage process [45]. However, these surface nickel oxide species can be reduced mostly by hydrogen during the catalytic hydrogenation (Fig. S3). After the introduction of Sn (Fig. 2b), the main peaks of Ni $2p_{3/2}$ for Ni_3Sn_2/TiO_2 and Ni_3Sn_2-ReO_x/TiO_2 shift to lower positions at 854.7 and 854.5 eV, respectively, in comparison to that of Ni/TiO_2 (855.1 eV). Meanwhile, the main peaks of Sn $3d_{5/2}$ of Ni_3Sn_2/TiO_2 and Ni_3Sn_2-ReO_x/TiO_2 shift to higher binding energies (486.2 and 486.6 eV) in comparison to the standard spectrum of Sn (486.0 eV). These results indicate that a significant electron donor from Sn to Ni exists, which would endow Ni with rich electron density for catalysis. In the fitting of Re 4 f spectrum of Ni_3Sn_2-ReO_x/TiO_2 (Fig. 2c, Table S4), the dominant peaks (72.3 %) located at 45.7 and 47.6 eV are attributed to Re^{6+}, which is accompanied by low percentages of Re^{4+}(14.1 %), Re^{3+} (8.4 %) and Re^0 (5.2 %) on the support. The rich $Re^{\delta+}$ species in Ni_3Sn_2-ReO_x/TiO_2

can be served as Lewis acid and strengthen the acidity of the catalyst [42].

SEM images (Fig. 3a) clearly show the spherical structure of nano-TiO_2 after loading Ni_3Sn_2-ReO_x. TEM images (Fig. 3b) show that Ni_3Sn_2 alloy NPs are highly dispersed on the support with an average size of 22.4 nm, clear lattice spacings of Ni_3Sn_2 alloy (d_{101} = 0.296 nm, d_{102} = 0.208 nm) and TiO_2 (d_{101} = 0.350 nm) are observed from the HRTEM images (Fig. 3c and d) of Ni_3Sn_2-ReO_x/TiO_2. EDS analysis (Fig. 3e) of Ni_3Sn_2-ReO_x/TiO_2 also reveals that Ni, Sn and Re elements are homogeneously distributed over the catalyst surface, which is also verified by EDS element surface scanning (Fig. S4 and S5). Comparatively, Ni NPs are well-dispersed in Ni/TiO_2, and the mean size of Ni NPs in Ni/TiO_2 is calculated to be 7.2 nm (Fig. S6). The larger size of Ni_3Sn_2 alloy NPs can be ascribed to the low Tammann temperature of Sn that results in the migration of Ni species during the catalyst reduction [46]. The AC STEM-HAADF image and elemental linear scanning of ReO_x/TiO_2 (Fig. S7) show that the widely dispersed ReO_x clusters (< 1 nm) are observed on the surface of TiO_2, accompanied by a small amount of atomic ReO_x. Based on the above observations, we can reasonably speculate that ReO_x is well-dispersed and interact intimately with Ni_3Sn_2 on the surface of the catalyst.
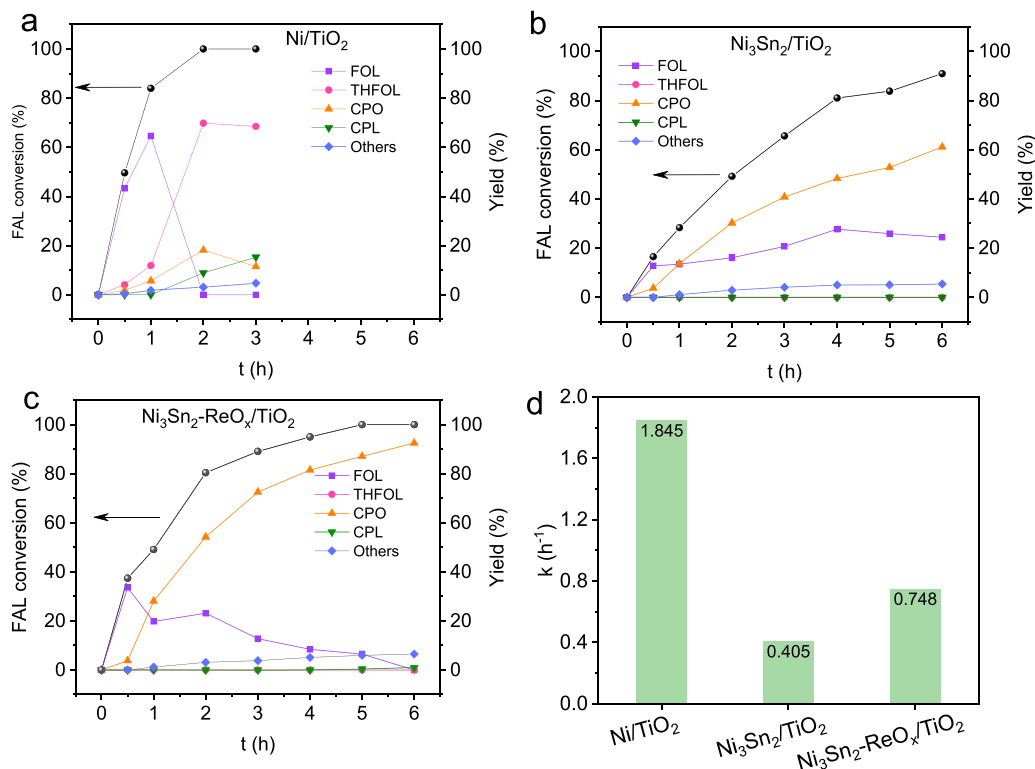
Fig. 4. (a-c) Time courses and (d) reaction rate constants of FAL hydrogenation over Ni/TiO$_2$, Ni$_3$Sn$_2$/TiO$_2$ and Ni$_3$Sn$_2$-ReO$_x$/TiO$_2$. Reaction conditions: FAL (1 mmol), catalyst (50 mg), H$_2$O (3.5 mL), H$_2$ (3 MPa), 140 °C.
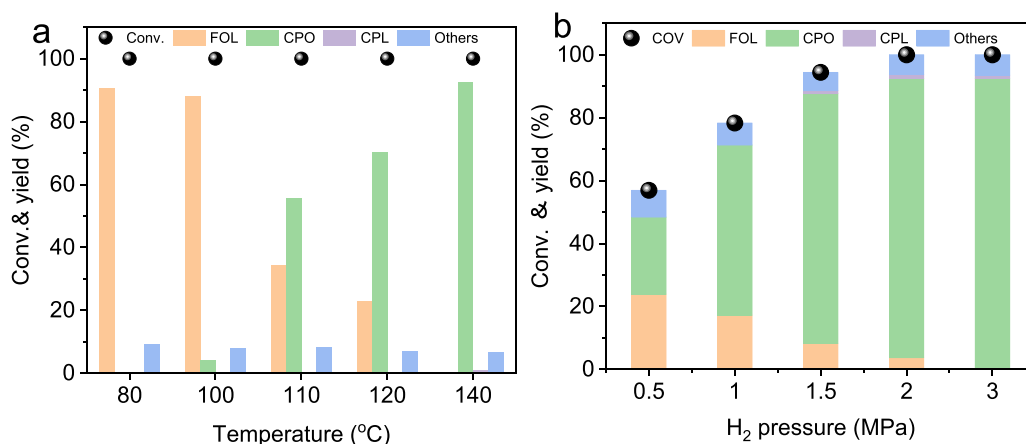

Fig. 5. The effects of (a) reaction temperature and (b) hydrogen pressure on furfural hydrogenation over Ni$_3$Sn$_2$-ReO$_x$/TiO$_2$. Reaction conditions: FAL (1 mmol), Ni$_3$Sn$_2$-ReO$_x$/TiO$_2$ (50 mg), H$_2$O (3.5 mL), H$_2$ (3 MPa), 140 °C, 6 h.

3.2. Catalyst performance for FAL hydrogenation

To evaluate the performance of as-obtained catalysts, FAL hydrogenation was selected as the probe reaction at 140 °C and 3 MPa H$_2$ (Table 1). When the FAL conversion of Ni/TiO$_2$ achieves 100 % at 3 h, the yields of THFOL, CPO and CPL are 68.5 %, 11.5 %, and 15.3 %, respectively (entry1). After the introduction of Sn, although the FAL conversion of Ni$_3$Sn$_2$/TiO$_2$ decreases to 65.6 %, the formation of THFOL is completely restrained, and the CPO yield reaches 40.8 % (entry 2). The Ni$_3$Sn$_2$-ReO$_x$/TiO$_2$ obtained by further doping ReO$_x$ achieves higher FAL conversion (89.1 %) and CPO yield (72.5 %) (entry 3). To elucidate the role of ReO$_x$, Ni-ReO$_x$/TiO$_2$ is prepared by doping ReO$_x$ on Ni/TiO$_2$, the FAL conversion remains 100 %, while the yields of THFOL, CPO and CPL are 41.2 %, 0 %, and 54.7 %, respectively (entry 4, Fig. S8). In

contrast, Ni$_3$Sn$_2$-ReO$_x$/TiO$_2$ exhibits good performance and achieves 100 % conversion and 92.5 % CPO yield when prolonging reaction time to 6 h (entry 7, Fig. 4c), which is much better than that of Ni/TiO$_2$ (100 % FAL conversion, 0 % CPO yield, entry 5) and Ni$_3$Sn$_2$/TiO$_2$ (90.9 % FAL conversion, 61.1 % CPO yield, entry 6). These results reveal that alloying Ni with Sn restrains the over-hydrogenation of the furan ring, while ReO$_x$ promotes the rearrangement of FOL and subsequent formation of CPO due to its Lewis acidity.

With Ni$_3$Sn$_2$-ReO$_x$/TiO$_2$ as the optimal catalyst, the influence of reaction temperature on FAL hydrogenation was studied in Fig. 5a. The conversion of FAL is nearly 100 %, the main product is FOL, and no CPO is obtained when the reaction temperature is 80 °C. As the reaction temperature increases, the yield of CPO increases, and the highest CPO yield is 92.5 % at 140 °C. When the reaction temperature is higher than
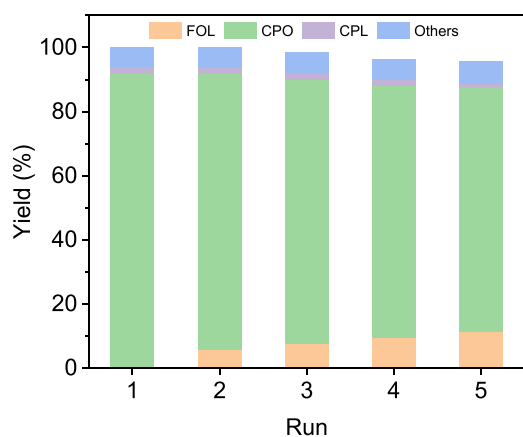
Fig. 6. Catalyst recyclability for FAL hydrogenation. Reaction conditions: FAL (1 mmol), Ni_3Sn_2-ReO_x/TiO_2 (50 mg), H_2O (3.5 mL), H_2 (3 MPa), 140 °C, 6 h.

140 °C, a minor of CPO is over-hydrogenated to CPL. Therefore, 140 °C is selected as the optimal reaction temperature for further investigations. The H_2 pressure is also a sensitive factor for FAL conversion (Fig. 5b). 56.9 % FAL conversion with 24.5 % CPO yield are obtained at 0.5 MPa H_2. Particularly, the yield of CPO increases with increasing the H_2 pressure, and reaches the maximum value (92.5 %) at 3.0 MPa H_2. When reaction time is prolonged to 18 h at 80 °C@3 MPa H_2 or 140 °C@0.5 MPa H_2 (Fig. S9), the yield of CPO can reach 85.3 % and 87.9 %, respectively, in the presence of full FAL conversion. Interestingly, by comparing the performance of the prepared bifunctional Ni_3Sn_2-ReO_x/TiO_2 catalyst with those based on noble/non-noble metal catalysts reported in the literature (Table S5), the promising performance of the synthesized catalyst for the selective hydrogenation of FAL into CPO in the moderate reaction conditions is observed. As listed in

Table S5, the catalytic FAL hydrogenation using Ni_3Sn_2-ReO_x/TiO_2 catalyst demonstrates almost higher CPO selectivity than those systems that used non-noble catalysts, which is the crucial factor from a laboratory/industry point of view. Additionally, the reaction is performed under milder reaction conditions (lower temperature and lower H_2 pressure) compared to most of the systems that applied noble and non-noble catalysts; consequently, this reveals the efficiency of the proposed catalytic reaction in this study.

The reusability of the Ni_3Sn_2-ReO_x/TiO_2 is performed at 140 °C for 6 h (Fig. 6). After five times recycling, the FAL conversion decreases slightly from 100 % to 95.9 %, and the yield of CPO decreases from 92.5 % to 76.4 %. The spent catalyst is characterized by XRD and XPS (Fig. S10), the crystalline phase of Ni_3Sn_2 is preserved, and the Ni 2p and Sn 3d peaks are almost unchanged, indicating NiSn is stable under the reaction conditions. However, the Re 4 f XPS spectra (Fig. S10a) show that partial Re species are reduced to lower valence Re (e.g., Re^0 and Re^{3+}) after recycling, which should be the primary cause of slight activity loss of the catalyst. Overall, these reaction results indicate that the Ni_3Sn_2-ReO_x/TiO_2 catalyst is reusable under the current reaction conditions.

3.3. Study of the reaction mechanism

To obtain more information about the reaction process and the roles of the catalyst during the reaction, using FOL as the substrate was performed for comparison (Fig. 7). The transformation of FOL on Ni/TiO_2 indicates that the mono-metallic Ni shows a high hydrogenation activity (k = 2.464 h^{-1}), but the THFOL is detected as sole product. While Ni_3Sn_2/TiO_2, shows a weak hydrogenation activity (k = 0.904 h^{-1}), CPO is the main product accompanied by ~5 % THFOL. For Ni_3Sn_2-ReO_x/TiO_2, the hydrogenation rate (k = 0.988 h^{-1}) is slightly higher than that of Ni_3Sn_2/TiO_2, but CPO is detected as the sole product. These
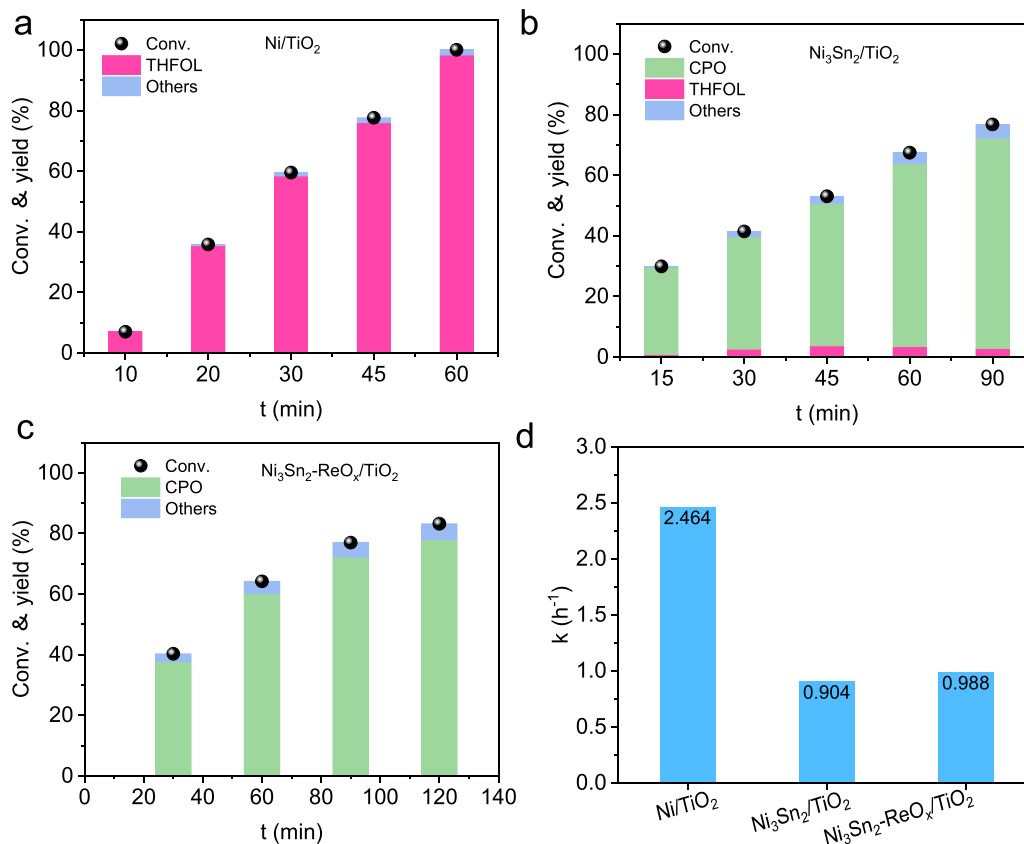

Fig. 7. (a-c) Time courses and (d) reaction rate constants of FOL hydrogenation over Ni/TiO_2, Ni_3Sn_2/TiO_2 and Ni_3Sn_2-ReO_x/TiO_2. Reaction conditions: substrate (1 mmol), catalyst (50 mg), H_2O (3.5 mL), H_2 (3 MPa), 140 °C.
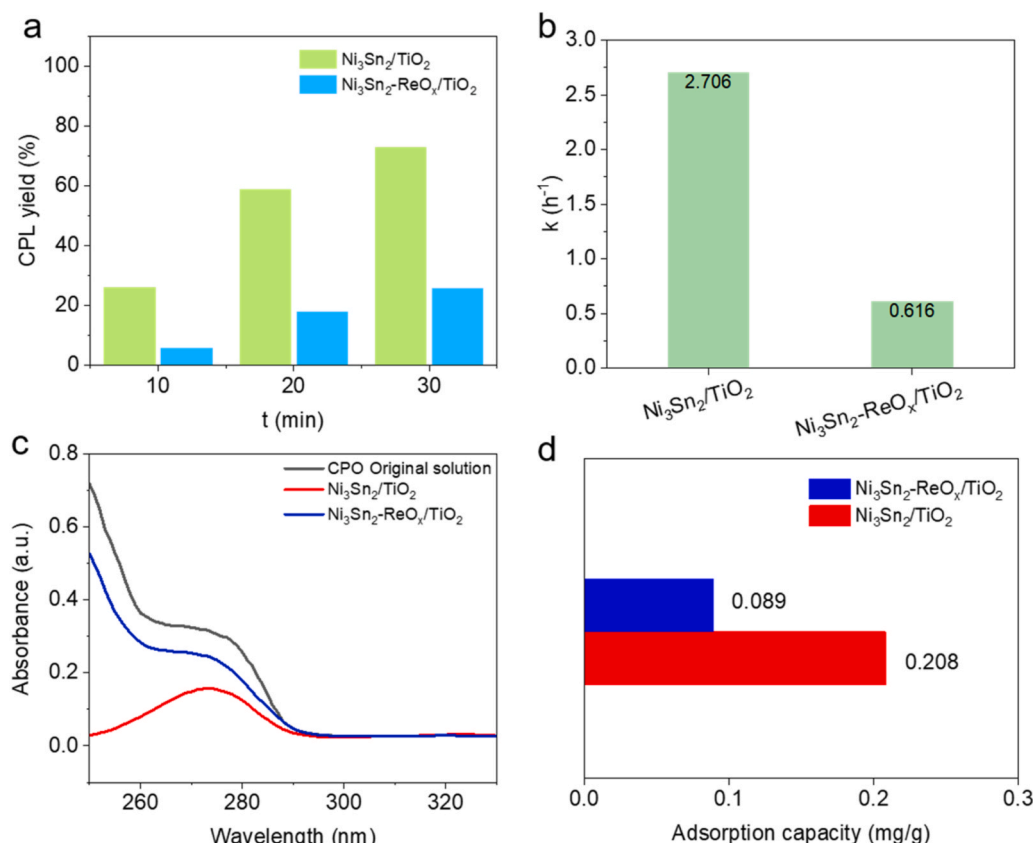
Fig. 8. (a) Time courses and (b) reaction rate constants of CPO hydrogenation over Ni$_3$Sn$_2$/TiO$_2$ and Ni$_3$Sn$_2$-ReO$_x$/TiO$_2$; (c) Adsorption profiles of CPO on Ni$_3$Sn$_2$/TiO$_2$ and Ni$_3$Sn$_2$-ReO$_x$/TiO$_2$ determined by UV–vis; (d) Saturated adsorption capacity of CPO on Ni$_3$Sn$_2$/TiO$_2$ and Ni$_3$Sn$_2$-ReO$_x$/TiO$_2$. Reaction conditions: substrate (1 mmol), catalyst (50 mg), H$_2$O (3.5 mL), H$_2$ (3 MPa), 140 °C.

results indicate that the hydrogenation and rearrangement of the furan ring are two parallel competing reactions on Ni-based catalysts [34], ReO$_x$ can act as acidic site and prefer to catalyze the rearrangement of FOL to CPO.

Moreover, the hydrogenations of CPO over Ni$_3$Sn$_2$/TiO$_2$ and Ni$_3$Sn$_2$-ReO$_x$/TiO$_2$ catalysts were also performed. As shown in Fig. 8a and b, compared with Ni$_3$Sn$_2$/TiO$_2$ (k = 2.706 h^{-1}), Ni$_3$Sn$_2$-ReO$_x$/TiO$_2$ shows a quite low CPO hydrogenation activity (k = 0.616 h^{-1}). To further explore the different activity of Ni$_3$Sn$_2$/TiO$_2$ and Ni$_3$Sn$_2$-ReO$_x$/TiO$_2$ catalysts, the adsorption capacity of Ni$_3$Sn$_2$/TiO$_2$ and Ni$_3$Sn$_2$-ReO$_x$/TiO$_2$ for CPO was determined by UV–vis experiment in Fig. 8c and d. It can be found that the adsorption capacity of CPO on Ni$_3$Sn$_2$-ReO$_x$/TiO$_2$ is 0.089 mg/g, which is much lower than that on Ni$_3$Sn$_2$/TiO$_2$ (0.208 mg/g). These results indicate ReO$_x$ is unfavorable to the adsorption of CPO on Ni$_3$Sn$_2$ surface, which can restrain the over-hydrogenation of CPO on Ni$_3$Sn$_2$-ReO$_x$/TiO$_2$.

To further explore the structural details of these Ni-based catalysts, in situ FTIR of CO absorption was performed. As shown in Fig. 9a, the signals at 2055 cm^{-1}, 2034 cm^{-1} and 2012 cm^{-1} are attributed to CO linear-type absorption on Ni NPs, while the signals at 1985 cm^{-1} and 1954 cm^{-1} are attributed to CO bridging-type absorption on Ni NPs [47]. For Ni/TiO$_2$, both CO linear and bridging-type absorptions are observed; while only signals of CO linear bonding can be observed for Ni$_3$Sn$_2$/TiO$_2$ and Ni$_3$Sn$_2$-ReO$_x$/TiO$_2$. This result indicates the introduction of Sn disturbs the atomic arrangement of Ni and separates continuous Ni sites, which could alter the adsorption configuration of furan ring on Ni surface [45].

To further study the adsorption behavior of FAL on the surface of catalysts, in situ FT-IR spectra were performed in Fig. 9b. As for FAL adsorption on mono-metallic Ni/TiO$_2$, a strong peak at 1582 cm^{-1} attributed to v(C═O) is observed, and another weak peak at 1354 cm^{-1}

is due to furan ring breath. Compared with gas phase furfural [48], the red-shift of v(C═O) and weakened furan ring breath indicate both C═O bond and furan ring undergo chemisorption on the surface of Ni (most likely parallel adsorption configuration) [45]. In the case of Ni$_3$Sn$_2$/-TiO$_2$, the v(C═O) band (1581 cm^{-1}) further weakens while the band of furan ring shows a rather weak intensity. This indicates that the adsorption of C═O bond enhances but that of furan ring weakens relative to pristine Ni. In the case of Ni$_3$Sn$_2$-ReO$_x$/TiO$_2$ however, the v(C═O) becomes negligible and the band of furan ring red-shifts to 1409 cm^{-1}, implying significantly promoted C═O activation and dramatically inhibited adsorption of furan ring. The results above confirm different adsorption configurations of FAL molecule on the surface of three catalysts, which would cause different reaction routes (Fig. 9d).

H$_2$-TPD test was used to study the dissociative adsorption of hydrogen on nickel-based catalysts (Fig. 9c). It can be seen that the desorption peaks of H$_2$ on Ni/TiO$_2$ appear at 120 °C and 390 °C. For Ni$_3$Sn$_2$/TiO$_2$, the former H$_2$ desorption peak is weakened, and the later one almost disappears, indicating that the incorporation of Sn results in a decrease of the H$_2$ activation ability of Ni, well agreed with the low reaction rate of FAL on Ni$_3$Sn$_2$/TiO$_2$ (Fig. 4d). After further incorporation of ReO$_x$, the second H$_2$ desorption peak of Ni$_3$Sn$_2$-ReO$_x$/TiO$_2$ is strengthened, ascribing to enhanced H$_2$ spillover induced by Lewis acidic ReO$_x$ [42].

Periodic DFT calculations were further performed on Ni and Ni$_3$Sn$_2$ to elucidate active sites and adsorption modes (Fig. 10). In the case of the most preferential Ni (111) facet, both FAL and FOL are bridge adsorbed on the top site of Ni and the furan ring is adsorbed with a parallel configuration on the surface across 3-fold hollow sites, illustrating the furan ring undergoes activation adsorption. The calculated adsorption energies of the FAL and FOL molecules on Ni (111) are −4.09
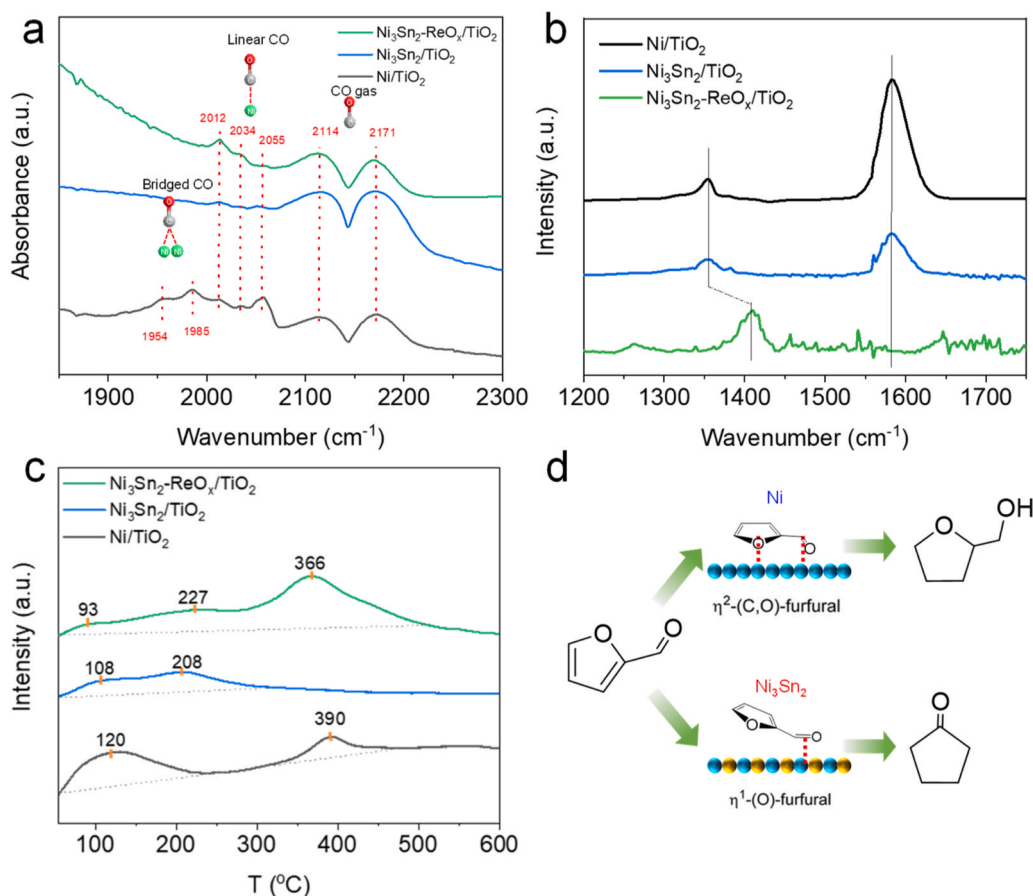
Fig. 9. (a) CO-DRIFT spectra, (b) in-situ FTIR spectra, (c) H_2-TPD spectra of Ni/TiO$_2$, Ni$_3$Sn$_2$/TiO$_2$ and Ni$_3$Sn$_2$-ReO$_x$/TiO$_2$, (d) adsorption model of FAL on Ni and Ni$_3$Sn$_2$ surfaces.
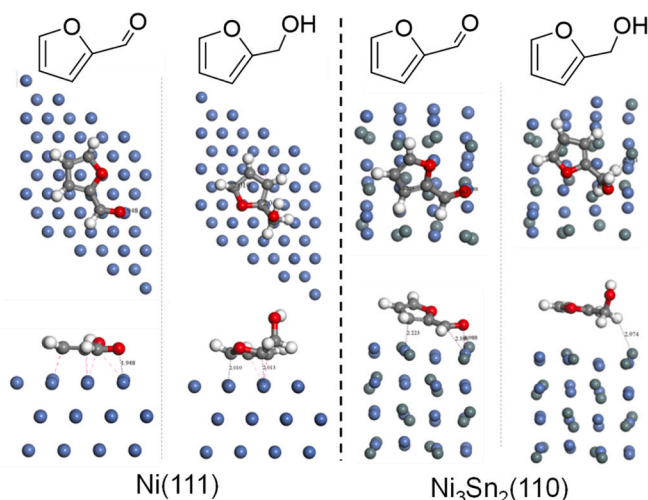

Fig. 10. Structure models for FAL and FOL adsorption on Ni (111) and Ni$_3$Sn$_2$(110) surfaces.

and −3.86 eV, respectively (Fig. 11a). As for Ni$_3$Sn$_2$ interface, the frequent (110) facet is chosen for FAL and FOL adsorption. it is found that the calculated adsorption energies of the FAL (−2.53 eV) and FOL (−1.22 eV) on Ni$_3$Sn$_2$ (110) are much lower than those on Ni (111). For instance, on the zigzag Ni$_3$Sn$_2$ (110) surface, the FAL and FOL molecules adsorbed on Ni$_3$Sn$_2$ (110) are interacted via -CH=O or -CH$_2$OH groups, Sn disturbs the atomic arrangement of Ni NPs and makes furan ring away from Ni atom. Similarly, the adsorption energies of FAL and FOL on Ni$_3$Sn$_2$ (101) and (102) surfaces are still lower than that of Ni (111)

(Figs. S11 and S12). The relatively weak adsorption energy on Ni$_3$Sn$_2$ surfaces may consequently weaken the furan ring adsorption and finally shifts the selectivity of FAL hydrogenation [49].

To further explore the reaction mechanism, FOL is used as the reactant in a water-solvent medium under N$_2$ atmosphere (Fig. 11b). Compared with catalyst-free and Ni/TiO$_2$-containing systems, the Ni$_3$Sn$_2$-ReO$_x$/TiO$_2$ with a strong Lewis acidity exhibits a much higher selectivity of 4-hydroxy-2-cyclopentenone (HCP) intermediate, indicating ReO$_x$ favors the ring-rearrangement of FOL. Based on the above theoretical calculation and controlled experiments, it is inferred that the role of Ni$_3$Sn$_2$ is to dissociate hydrogen and that the role of ReO$_x$ is to bind and activate the substrate (Fig. 12). When the catalyst contains both Ni$_3$Sn$_2$ and ReO$_x$, the hydrogenation pathway of furfural may be as follows: the C=O bond of FAL is preferentially adsorbed on Ni$_3$Sn$_2$ surface, then hydrogenated into FOL by H atoms bonded on Ni$_3$Sn$_2$. The as-formed FOL is activated by Lewis acid ReO$_x$ and rearranged into HCP, then HCP is hydrogenated and dehydrated into 2-cyclopentenone (CPEO) by the synergy of Ni$_3$Sn$_2$ and ReO$_x$[18]. Finally, CPO is obtained by hydrogenation of CPEO over Ni$_3$Sn$_2$, followed by its desorption (Fig. 12).

4. Conclusion

In summary, Ni$_3$Sn$_2$-ReO$_x$/TiO$_2$ catalyst was prepared by continuous impregnation method and applied for selective FAL hydrogenation to CPO. At 140 °C and 3 MPa H$_2$ for 6 h, the FAL conversion and CPO selectivity are 100 % and 92.5 %, respectively, on Ni$_3$Sn$_2$-ReO$_x$/TiO$_2$, which are much higher than Ni/TiO2 and Ni$_3$Sn$_2$/TiO$_2$ catalysts. The transformation of FAL to CPO involves the selective hydrogenation of the C=O bond and FOL rearrangement on Ni$_3$Sn$_2$-ReO$_x$/TiO$_2$, which
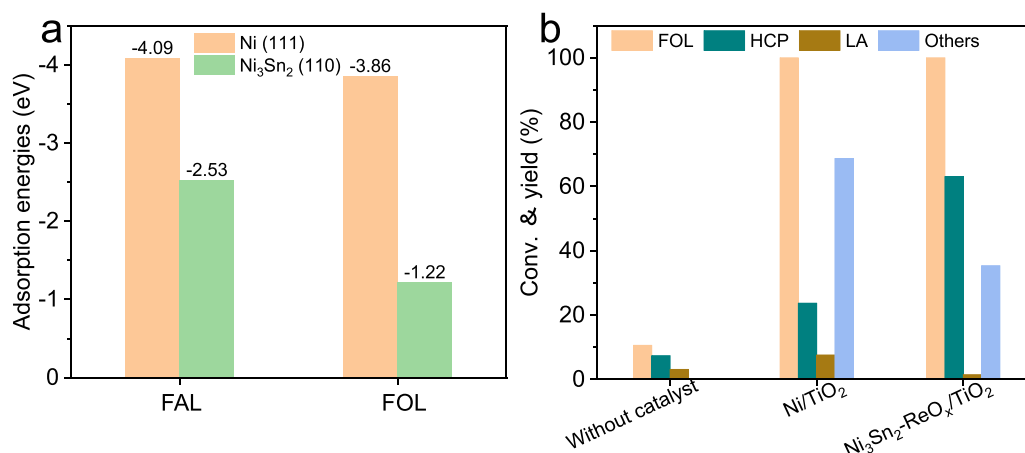
Fig. 11. (a) Adsorption energies of FAL and FOL on Ni (111) and Ni₃Sn₂ (110) surfaces, (b) catalytic performance of FOL reaction over various catalysts. Reaction conditions: FOL (1 mmol), catalyst (50 mg), H₂O (3.5 mL), N₂ (3 MPa), 140 °C, 3 h.
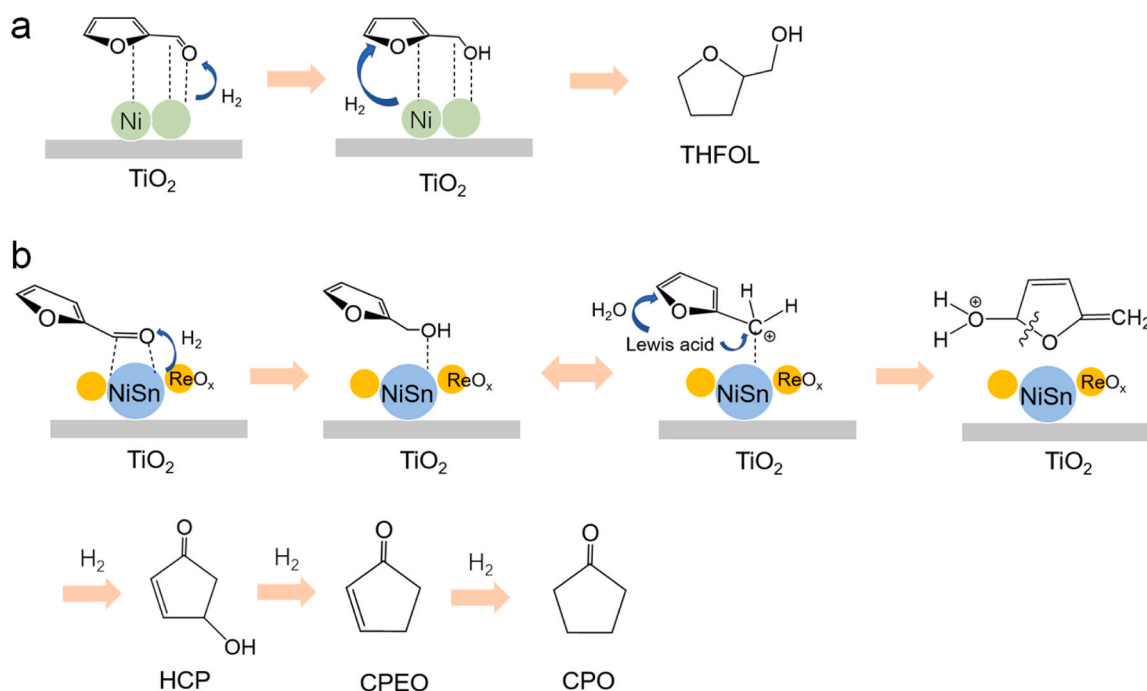

Fig. 12. Schematic reaction mechanism of FAL hydrogenation to CPO over Ni₃Sn₂-ReOₓ/TiO₂ catalyst.

strongly depends on the synergistic effect between the Ni₃Sn₂ NPs and ReOx species. Wide characterizations reveal that the Ni₃Sn₂ inhibits the over-hydrogenation of furan ring, which significantly shifts the reaction routine; while the doping of oxyphilic ReOₓ promotes both the C-O bond activation and the hydrogen activation on the catalyst, thus accelerating the overall reaction rate. DFT calculations show that FAL is adsorbed parallelly on Ni surface, while adsorbed slantly on Ni3Sn2 surface. Moreover, the catalyst is recyclable for five times and also active at even 0.5 MPa H2 and 80 °C. These results demonstrate the feasibility of the practical CPO production from biomass resources by designing and optimizing the composition and structure of catalyst.

CRediT authorship contribution statement

R.N. designed the experiments. R.N. and Y.X.Z. supervised the project. W.L. performed the experiments. All authors discussed the experiments and results. R.N., Y.X.Z., X. L., and W. L. prepared and revised the manuscript.

Declaration of Competing Interest

The authors declare no competing financial interest.

Data availability

No data was used for the research described in the article.

University for FTIR test.

Appendix A. Supporting information

Supplementary data associated with this article can be found in the online version at doi:10.1016/j.apcatb.2023.123191.

References

[1] P. Gallezot, Conversion of biomass to selected chemical products, Chem. Soc. Rev. 41 (2012) 1538–1558.
[2] Y. Yang, Z. Du, Y. Huang, F. Lu, F. Wang, J. Gao, J. Xu, Conversion of furfural into cyclopentanone over Ni–Cu bimetallic catalysts, Green. Chem. 15 (2013) 1932–1940.
[3] T. Akashi, S. Sato, R. Takahashi, T. Sodesawa, K. Inui, Catalytic vapor-phase cyclization of 1,6-hexanediol into cyclopentanone, Catal. Commun. 4 (2003) 411–416.
[4] W. Gong, C. Chen, H. Zhang, G. Wang, H. Zhao, In situ synthesis of highly dispersed Cu–Co bimetallic nanoparticles for tandem hydrogenation/rearrangement of bioderived furfural in aqueous-phase, ACS Sustain. Chem. Eng. 6 (2018) 14919–14925.
[5] M. Renz, Ketonization of carboxylic acids by decarboxylation: mechanism and scope, Eur. J. Org. Chem. 2005 (2005) 979–988.
[6] W. Cai, Y. Li, Q. Zheng, M. Song, P. Ma, W. Fang, W. Song, W. Lai, Hydrogenative rearrangement of bioderived furfurals to cyclopentanones over Ni/Nb$_2$O$_5$ catalysts: promotion effect of reducible NbO$_x$ and water, Fuel 338 (2023) 127345.
[7] K.A. Dubkov, G.I. Panov, E.V. Starokon, V.N. Parmon, Non-catalytic liquid phase oxidation of alkenes with nitrous oxide. 2. Oxidation of cyclopentene to cyclopentanone, React. Kinet. Catal. Lett. 77 (2002) 197–205.
[8] R. Balaga, P. Balla, X. Zhang, K. Ramineni, H. Du, S. Lingalwar, V. Perupogu, Z. C. Zhang, Enhanced cyclopentanone yield from furfural hydrogenation: promotional effect of surface silanols on Ni-Cu/m-silica catalyst, Catalysts 13 (2023) 580–597.
[9] Z. Hu, M. Han, C. Chen, Z. Zou, Y. Shen, Z. Fu, X. Zhu, Y. Zhang, H. Zhang, H. Zhao, G. Wang, Hollow carbon sphere encapsulated nickel nanoreactor for aqueous-phase hydrogenation-rearrangement tandem reaction with enhanced catalytic performance, Appl. Catal. B 306 (2022) 121140.
[10] Z. Hu, A. Xie, C. Chen, Z. Zou, Y. Shen, Z. Fu, Y. Zhang, H. Zhang, H. Zhao, G. Wang, Facile synthesis of N, P co-doped carbon encapsulated Ni catalyst for green production of cyclopentanone from biomass derivative furfural, Fuel 319 (2022), 123815.
[11] W. Gong, C. Chen, H. Zhang, G. Wang, H. Zhao, Highly dispersed Co and Ni nanoparticles encapsulated in N-doped carbon nanotubes as efficient catalysts for the reduction of unsaturated oxygen compounds in aqueous phase, Catal. Sci. Technol. 8 (2018) 5506–5514.
[12] D. Wang, M. Al-Mamun, W. Gong, Y. Lv, C. Chen, Y. Lin, G. Wang, H. Zhang, H. Zhao, Converting Co^{2+}-impregnated g-C$_3$N$_4$ into N-doped CNTs-confined Co nanoparticles for efficient hydrogenation rearrangement reactions of furanic aldehydes, Nano Res. 14 (2021) 2845–2852.
[13] C. Xu, E. Paone, D. Rodríguez-Padrón, R. Luque, F. Mauriello, Recent catalytic routes for the preparation and the upgrading of biomass derived furfural and 5-hydroxymethylfurfural, Chem. Soc. Rev. 49 (2020) 4273–4306.
[14] Y. Shao, J. Wu, Z. Zheng, M. Fan, K. Sun, F.M. Bkangmo Kontchouo, L. Zhang, S. Zhang, G. Hu, X. Hu, Alloying cobalt in Co–Fe–Al catalyst for achieving the selective conversion of furfural to cyclopentanone, Renew, Energ 195 (2022) 957–971.
[15] Y. Tian, B. Chen, Z. Yu, R. Huang, G. Yan, Z. Li, Y. Sun, S. Yang, X. Tang, L. Lin, X. Zeng, Efficient catalytic hydrogenation of furfural over cobalt-based catalysts with adjustable acidity, Chem. Eng. Sci. 270 (2023), 118527.
[16] R. Fang, H. Liu, R. Luque, Y. Li, Efficient and selective hydrogenation of biomass-derived furfural to cyclopentanone using Ru catalysts, Green. Chem. 17 (2015) 4183–4188.
[17] J. Lee, J. Woo, C. Nguyen-Huy, M.S. Lee, S.H. Joo, K. An, Highly dispersed Pd catalysts supported on various carbons for furfural hydrogenation, Catal. Today 350 (2020) 71–79.
[18] Q. Deng, R. Gao, X. Li, J. Wang, Z. Zeng, J.-J. Zou, S. Deng, Hydrogenative ring-rearrangement of biobased furanic aldehydes to cyclopentanone compounds over Pd/pyrochlore by introducing oxygen vacancies, ACS Catal. 10 (2020) 7355–7366.
[19] M. Hronec, K. Fulajtárová, Selective transformation of furfural to cyclopentanone, Catal. Commun. 24 (2012) 100–104.
[20] X. Zhou, Z. Feng, W. Guo, J. Liu, R. Li, R. Chen, J. Huang, Hydrogenation and hydrolysis of furfural to furfuryl alcohol, cyclopentanone, and cyclopentanol with a heterogeneous copper catalyst in water, Ind. Eng. Chem. Res. 58 (2019) 3988–3993.
[21] P. Pan, W.-Y. Xu, T.-J. Pu, X.D. Wang, X.-J. Pei, F. Tang, Y.S. Feng, Selective conversion of furfural to cyclopentanone and cyclopentanol by magnetic Cu-Fe$_3$O$_4$ NPs catalyst, ChemistrySelect 4 (2019) 5845–5852.
[22] Y. Shao, K. Sun, M. Fan, G. Gao, J. Wang, L. Zhang, S. Zhang, X. Hu, Synthesis of a thermally and hydrothermally stable copper-based catalyst via alloying of Cu with Ni and Zn for catalyzing conversion of furfural into cyclopentanone, ACS Sustain. Chem. Eng. 10 (2022) 8763–8777.

[23] S. Chen, T.T. Qian, L.L. Ling, W. Zhang, B.B. Gong, H. Jiang, Hydrogenation of furfural to cyclopentanone under mild conditions by a structure-optimized Ni-NiO/TiO$_2$ heterojunction catalyst, ChemSusChem 13 (2020) 5507–5515.
[24] Z. Yu, H. Tian, K. Sun, Y. Shao, L. Zhang, S. Zhang, P. Duan, Q. Liu, S. Niu, D. Dong, X. Hu, Impacts of externally added Brønsted and Lewis acid on conversion of furfural to cyclopentanone over Ni/SiC catalyst, Mol. Catal. 496 (2020), 111187.
[25] M. Zhou, H. Zhu, L. Niu, G. Xiao, R. Xiao, Catalytic hydroprocessing of furfural to cyclopentanol over Ni/CNTs catalysts: model reaction for upgrading of bio-oil, Catal. Lett. 144 (2013) 235–241.
[26] Y.-F. Ma, H. Wang, G.-Y. Xu, X.-H. Liu, Y. Zhang, Y. Fu, Selective conversion of furfural to cyclopentanol over cobalt catalysts in one step, Chin. Chem. Lett. 28 (2017) 1153–1158.
[27] V. Ranaware, R.G. Kurniawan, D. Verma, S.K. Kwak, B.C. Ryu, J.W. Kang, J. Kim, Solvent-mediated selectivity control of furfural hydrogenation over a N-doped carbon-nanotube-supported Co/CoOx catalyst, Appl. Catal. B 318 (2022), 121838.
[28] H. Li, J. Liu, C. Cai, H. Wang, Y. Huang, C. Wang, L. Ma, Selectivity catalytic transfer hydrogenation of biomass-based furfural to cyclopentanone, Fuel 332 (2023), 126057.
[29] M.V. Twigg, M.S. Spencer, Deactivation of supported copper metal catalysts for hydrogenation reactions, Appl. Catal. A 212 (2001) 161–174.
[30] Y. Su, C. Chen, X. Zhu, Y. Zhang, W. Gong, H. Zhang, H. Zhao, G. Wang, Carbon-embedded Ni nanocatalysts derived from MOFs by a sacrificial template method for efficient hydrogenation of furfural to tetrahydrofurfuryl alcohol, Dalton Trans. 46 (2017) 6358–6365.
[31] Y. Wang, M. Zhou, T. Wang, G. Xiao, Conversion of furfural to cyclopentanol on Cu/Zn/Al catalysts derived from hydrotalcite-like materials, Catal. Lett. 145 (2015) 1557–1565.
[32] M. Hronec, K. Fulajtárová, I. Vávra, T. Soták, E. Dobročka, M. Mičušík, Carbon supported Pd–Cu catalysts for highly selective rearrangement of furfural to cyclopentanone, Appl. Catal. B 181 (2016) 210–219.
[33] Y. Wang, C. Liu, X. Zhang, One-step encapsulation of bimetallic Pd–Co nanoparticles within UiO-66 for selective conversion of furfural to cyclopentanone, Catal. Lett. 150 (2020) 2158–2166.
[34] X.-L. Li, J. Deng, J. Shi, T. Pan, C.-G. Yu, H.-J. Xu, Y. Fu, Selective conversion of furfural to cyclopentanone or cyclopentanol using different preparation methods of Cu–Co catalysts, Green. Chem. 17 (2015) 1038–1046.
[35] S. Zhang, H. Ma, Y. Sun, X. Liu, M. Zhang, Y. Luo, J. Gao, J. Xu, Selective tandem hydrogenation and rearrangement of furfural to cyclopentanone over CuNi bimetallic catalyst in water, Chin. J. Catal. 42 (2021) 2216–2224.
[36] M. Zhou, J. Li, K. Wang, H. Xia, J. Xu, J. Jiang, Selective conversion of furfural to cyclopentanone over CNT-supported Cu based catalysts: model reaction for upgrading of bio-oil, Fuel 202 (2017) 1–11.
[37] C. Chen, M. Zhou, J. Jiang, Selective aqueous-phase hydrogenation of furfural to cyclopentanol over Ni-based catalyst under mild conditions, J. Chin. Chem. Soc. 68 (2021) 1177–1180.
[38] T. Shen, R. Hu, C. Zhu, M. Li, W. Zhuang, C. Tang, H. Ying, Production of cyclopentanone from furfural over Ru/C with Al$_{11.6}$PO$_{23.7}$ and application in the synthesis of diesel range alkanes, RSC Adv. 8 (2018) 37993–38001.
[39] Q. Deng, R. Gao, X. Li, J. Wang, Z. Zeng, J.-J. Zou, S. Deng, Hydrogenative ring-rearrangement of biobased furanic aldehydes to cyclopentanone compounds over Pd/pyrochlore by introducing oxygen vacancies, ACS Catal. 10 (2020) 7355–7366.
[40] Q. Deng, R. Gao, Y.C. Zhang, X. Li, J. Li, S. Tu, G. Sheng, J. Wang, Z. Zeng, T. Yoskamtorn, S.C. Edman Tsang, H$^+$ -H$^-$ Pairs in partially oxidized MAX phases for bifunctional catalytic conversion of furfurals into linear ketones, Angew. Chem. Int Ed. Engl. 62 (2023), e202211461.
[41] R. Rodiansono, M. Dewi Astuti, T. Hara, N. Ichikuni, S. Shimazu, One-pot selective conversion of C5-furan into 1,4-pentanediol over bulk Ni–Sn alloy catalysts in an ethanol/H$_2$O solvent mixture, Green. Chem. 21 (2019) 2307–2315.
[42] J.H. Jang, I. Ro, P. Christopher, M.M. Abu-Omar, A heterogeneous Pt-ReO$_x$/C catalyst for making renewable adipates in one step from sugar acids, ACS Catal. 11 (2020) 95–109.
[43] M.P.B. Vega, M. Hinojosa-Reyes, A. Hernández-Ramírez, J.L.G. Mar, V. Rodríguez-González, L. Hinojosa-Reyes, Visible light photocatalytic activity of sol–gel Ni-doped TiO$_2$ on p-arsanilic acid degradation, J Solgel, Sci. Technol. 85 (2018) 723–731.
[44] J. Zhu, J. Ren, Y. Huo, Z. Bian, H. Li, Nanocrystalline Fe/TiO$_2$ visible photocatalyst with a mesoporous structure prepared via a nonhydrolytic sol-gel route, J. Phys. Chem. C 111 (2007) 18965–18969.
[45] Y. Zhang, A. Rezayan, K. Wang, J. Wang, C.C. Xu, R. Nie, On-demand, highly tunable, and selective 5-hydroxymethylfurfural hydrogenation to Furan Diols enabled by Ni and Ni$_3$Ga alloy catalysts, ACS Catal. 13 (2022) 803–814.
[46] V.S. Marakatti, N. Arora, S. Rai, S.C. Sarma, S.C. Peter, Understanding the role of atomic ordering in the crystal structures of Ni$_x$Sn$_y$ toward efficient vapor phase furfural hydrogenation, ACS Sustain. Chem. Eng. 6 (2018) 7325–7338.
[47] M. Mihaylov, K. Hadjiivanov, H. Knözinger, Formation of Ni(CO)$_4$ during the Interaction between CO and silica-supported nickel catalyst: an FTIR spectroscopic study, Catal. Lett. 76 (2001) 59–63.
[48] W. Liu, Y. Yang, L. Chen, E. Xu, J. Xu, S. Hong, X. Zhang, M. Wei, Atomically-ordered active sites in NiMo intermetallic compound toward low-pressure hydrodeoxygenation of furfural, Appl. Catal. B 282 (2021), 119569.
[49] S. Campisi, C.E. Chan-Thaw, L.E. Chinchilla, A. Chutia, G.A. Botton, K.M. H. Mohammed, N. Dimitratos, P.P. Wells, A. Villa, Dual-site-mediated hydrogenation catalysis on Pd/NiO: selective biomass transformation and maintenance of catalytic activity at low Pd loading, ACS Catal. 10 (2020) 5483–5492.